LRP 505/94 September 1994

ELECTRON CYCLOTRON RESONANCE HEATING

A. Pochelon

36th Course of the "Association Vaudoise des Chercheurs en Physique"

Lecture given at the
36th Course of the "Association Vaudoise des Chercheurs en Physique"
THE CHALLENGES OF MAGNETIC FUSION RESEARCH
21-26 March 1994, Grimentz, Valais
Switzerland

ELECTRON CYCLOTRON RESONANCE HEATING

A. Pochelon

Centre de Recherches en Physique des Plasmas
Association Euratom - Confédération Suisse
Ecole Polytechnique Fédérale de Lausanne
21, Av. des Bains, CH-1007 Lausanne, Switzerland

INTRODUCTION

With the availability of high frequency ($f \geq 50$ GHz) high power microwave sources, Electron Cyclotron Resonance Heating (ECRH) is widely used in present-day tokamaks and stellarators and is planned for applications in ITER (International Thermonuclear Experimental Reactor). ECRH can be used over a broad spectrum of applications ranging from heating, with the aim of increasing plasma temperature and pressure, to plasma profile tailoring, in particular current profile tailoring, with the aim of enhancing or optimising stability and confinement properties.

The presentation is structured as follows: the first points to be discussed when considering ECRH are accessibility (Chap. 1) and absorption (Chap. 2), although it will be seen that it is not easy to separate one from the other due to the links between absorption and propagation. Some examples of the use of ECRH as a tool for different physics applications in tokamaks will be addressed in Chap. 3. The applications envisioned for the Next Step (ITER) and for the Reactor will be the subject of Chap. 4.

1. RESONANCES AND CUTOFFS IN A TOKAMAK

There are two important aspects for the heating of a plasma: the accessibility and the dissipation. The accessibility depends mainly on the topology of wave cutoffs and the dissipation of the incoming wave is usually linked with the presence of a resonance. These situations can best be described using the Clemmow-Mullaly-Allis (CMA) diagram for a cold electron plasma, which is shown in Fig. 1. Let us remember the electron cyclotron frequency, defined as $\omega_{ce} = eB/m_e$, and the electron plasma frequency, defined as $\omega_{pe} = (n_e e^2/m_e \varepsilon_0)^{1/2}$. Therefore the horizontal axis represents essentially the density ($\sim n_e/\omega^2$) and the vertical axis the magnetic field ($\sim B_0^2/\omega^2$). The solid horizontal line at $\omega_{ce}^2/\omega^2 = 1$ represents the cyclotron resonance; the line labeled upper hybrid (UH) represents the upper hybrid resonance $\omega_{UH}^2 = \omega_{pe}^2 + \omega_{ce}^2$; and the line labeled "cutoff" between regions 1 and 4 represents the right-hand cutoff boundary for the *extraordinary wave* (*X-mode*, $\underline{E} \perp \underline{B_0}$), and is defined as:

$$\omega_R = \frac{\omega_{ce}}{2} + \left[\left(\frac{\omega_{ce}}{2}\right)^2 + \omega_{pe}^2\right]^{1/2}.$$

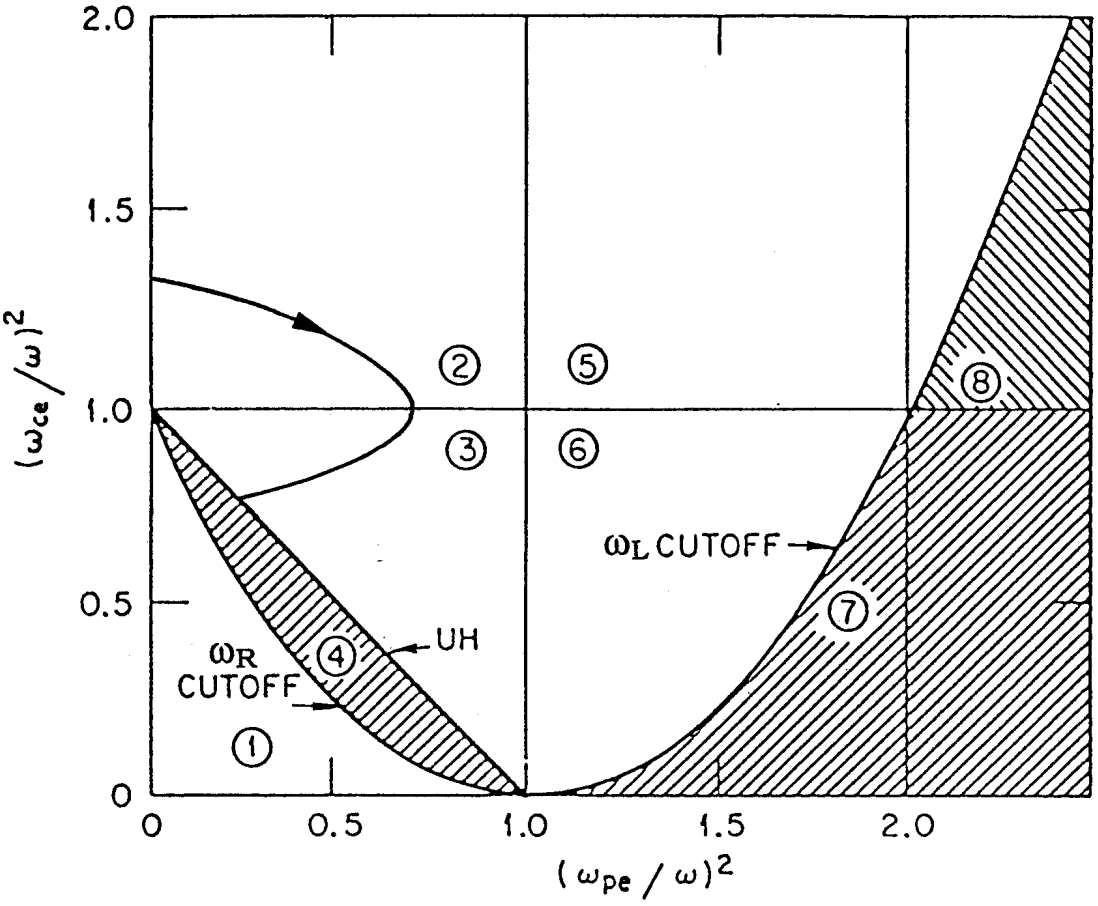

Fig. 1 - CMA diagram for Electron Cyclotron Waves

At the upper hybrid resonance (UHR), the index of refraction N goes to infinity ($N = kc/\omega = c/v_{phase} \rightarrow \infty$) and at a cutoff, such as ω_R, $N = 0$. At the cyclotron resonance, the value of N is finite and varies smoothly through the resonance. The thick trajectory shows a typical ray path for a launch from the high field side (HFS) of a tokamak, where the magnetic field is high and $\omega_{ce} \geq \omega$.

The *extraordinary wave* is cut off in region 4. If such a wave is launched from the low field side (LFS) [i.e., $(\omega_{ce}/\omega)^2 < 1$], it will encounter the ω_R cutoff at very low density, therefore close to plasma edge. The right-hand wave is absorbed near cyclotron resonance in regions 2 and 5. The left-hand wave can propagate in regions 1,2, and 3. The boundary between regions 6 and 7 is due to the left-hand cutoff

$$\omega_L = -\frac{\omega_{ce}}{2} + \left[\left(\frac{\omega_{ce}}{2}\right)^2 + \omega_{pe}^2\right]^{1/2}.$$

In high density cases the plasma centre is cut off to the extraordinary wave by this cutoff ω_L and no cold plasma wave can propagate in region 7.

To further clarify the points about fundamental heating in tokamak geometry, Fig. 2 illustrates the regions of propagation and evanescence for a typical tokamak geometry with the resonance located at the plasma

axis. Projected on the cross section are the cutoffs, resonances and evanescent regions for a) a low-density, b) a moderate-density and c) a high-density plasma for extraordinary wave propagation. Note that the ECR and UHR regions are always accessible from the high field side, except for high density cases where the plasma centre is not accessible due to the left-hand cutoff ω_L.

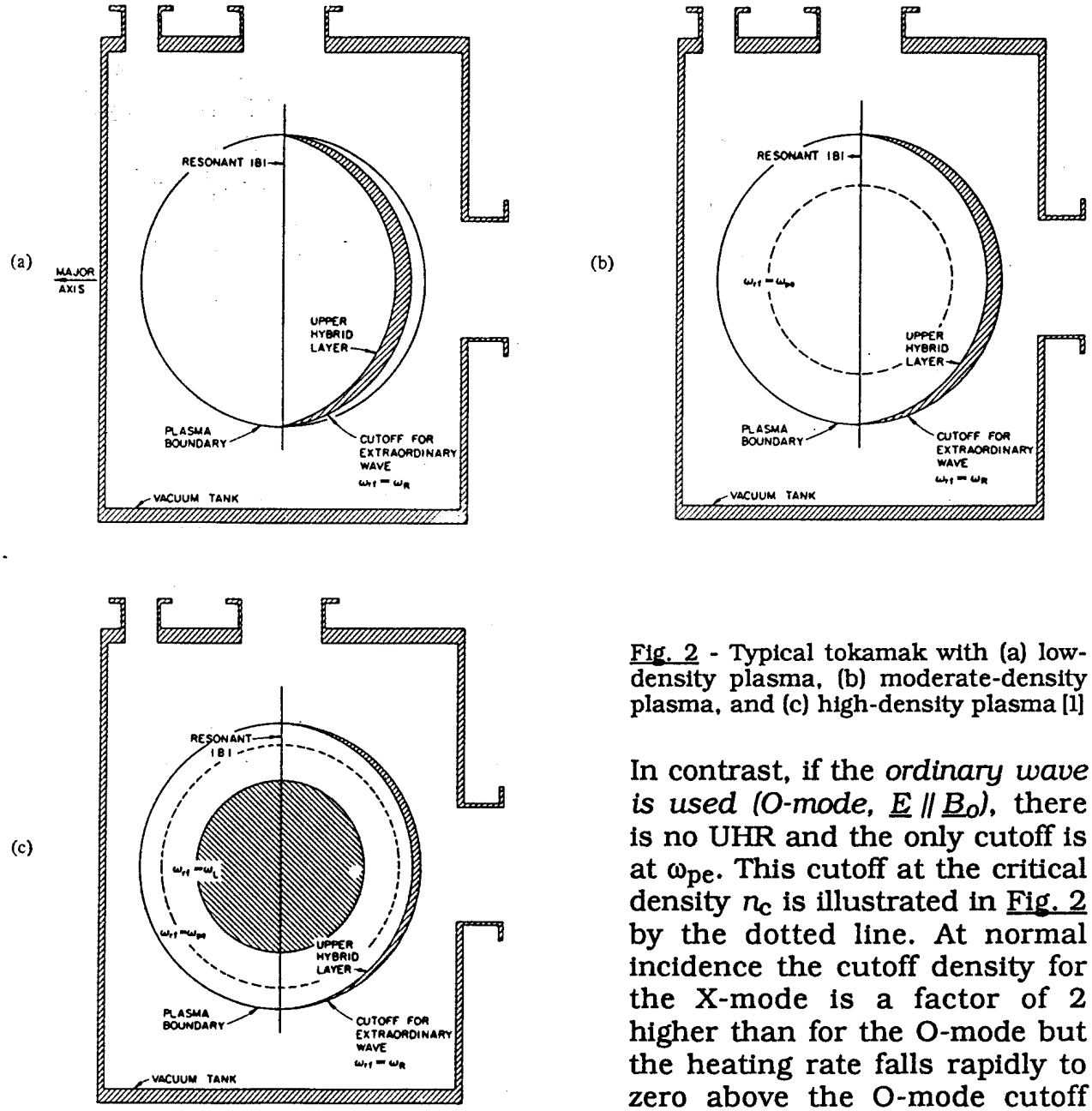

Fig. 2 - Typical tokamak with (a) low-density plasma, (b) moderate-density plasma, and (c) high-density plasma [1]

In contrast, if the *ordinary wave is used (O-mode, $\underline{E} \parallel \underline{B}_o$)*, there is no UHR and the only cutoff is at ω_{pe}. This cutoff at the critical density n_c is illustrated in Fig. 2 by the dotted line. At normal incidence the cutoff density for the X-mode is a factor of 2 higher than for the O-mode but the heating rate falls rapidly to zero above the O-mode cutoff density. In cold plasma theory, collisional damping of this wave is possible; in hot plasma theory, there is cyclotron damping, which is maximum for propagation normal to the confining magnetic field for O-mode. For X-mode at first harmonic, the absorption increases when deviating from the normal.

Heating at higher harmonics, at the second harmonic, $(\omega_{ce}/\omega)^2 = 0.25$ on the ordinate of Fig. 1, or at the third harmonic,

For appropriately chosen parameters the ECH waves are totally damped within a few centimetres of the cyclotron resonance. For quasi-horizontal launch and provided that the vertical spread of the incident RF power is small, this offers well-localised absorption in minor radius at readily adjustable position even in machines of modest minor cross section. The width of the absorption zone (in major radius) is determined by the strength of the interaction and the magnitudes of the relativistic and Doppler broadening terms.

1.2 Comparison with Experiments

1.2.1 Resonances Location

The ECRH breakdown experiments carried out in the CRPP-TCA tokamak showed particularly well the presence of the cyclotron resonance and the upper hybrid resonance [6]. The HFS antenna location in the vacuum vessel is shown in Fig. 3. It consists of a steering mirror which can launch the beam at various poloidal and toroidal angles. The antenna could launch either X- or O-mode, which for HFS launch can both access the resonance, as seen in the CMA diagram. During breakdown of the neutral gas with ECRH power, we used a vertically viewing H_α camera equipped with 128 radial channels, showing the details of the radial absorption layers.

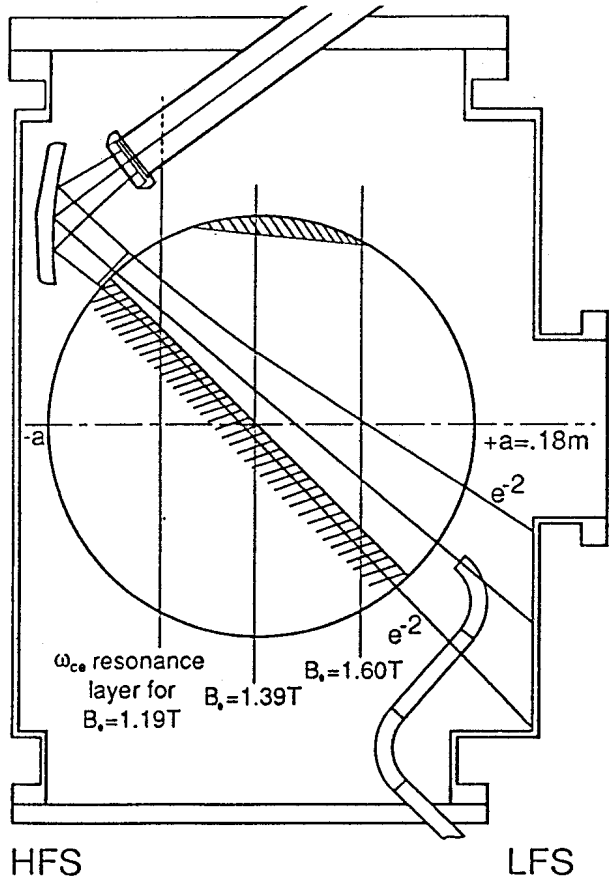

Fig. 3 - TCA poloidal cross section including waveguide, quartz window, ellipsoidal microwave mirror, and transmission measurement antennas. The mirror is steerable allowing access to the region between the cross-hatched lines. Toroidal angles of ±25° to the radial are also possible.

The H_α emission profiles show two distinct absorption peaks: the EC resonance and the UH layer on the LFS. The H_α emission profiles for X- and O-mode are superimposed in Fig. 4 . The EC resonance close to $x \equiv r/a \cong 0$ is well seen in O-mode, which has higher first-pass absorption for perpendicular injection than X-mode.

1.2.2 Cutoffs

The occurrence of the X- or O-mode cutoffs can be seen indirectly in heating experiments, while increasing the density. The experimentally determined efficiency of central heating of X1, O1, X2, on the DIII-D tokamak, measured as a function of density were compared to theoretical calculations of first pass absorption (using the TORAY ray tracing code [7]). In those experiments [8], it was found that the density at which the heating efficiency began to drop was consistent with theory and that heating at the highest densities was attained using HFS X-mode launch, as shown in Fig. 6. These inside launch results were corroborated by work on DITE, where increases in poloidal beta β_p were found up to the expected cutoff density, Fig. 7 [9].

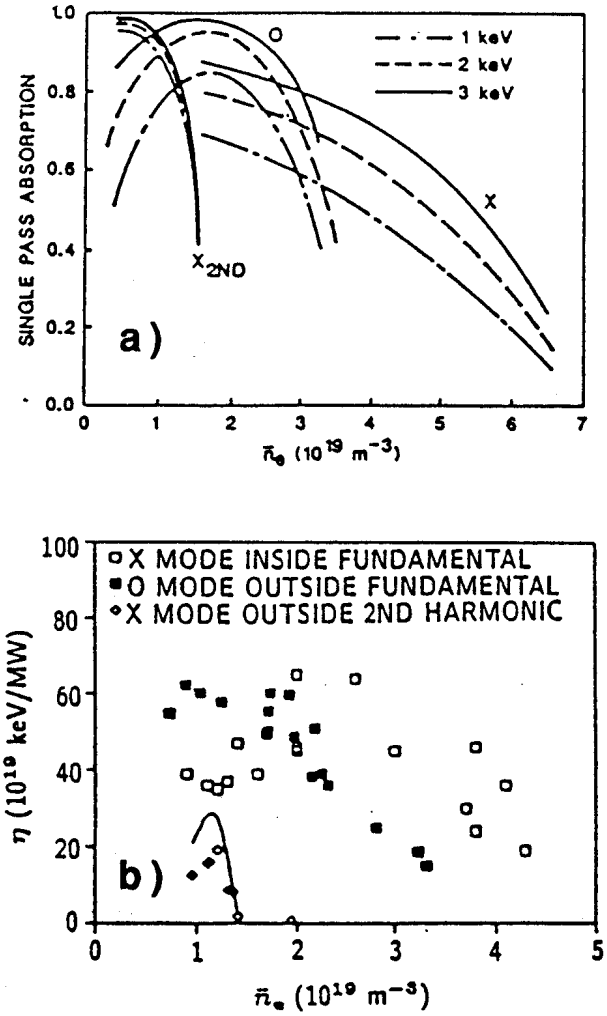

Fig. 6 - Calculated and observed heating effects for DIII-D, comparing fundamental X-mode (inside launch), fundamental O-mode (outside launch), and second harmonic X-mode (outside launch, same frequency, half the field).
In each case, the resonance is placed near the plasma axis. (a) First pass absorption calculations from the TORAY code; (b) heating efficiency $\eta = \bar{n}_e \Delta T_e(0) V / P_{ECH}$ as a function of line-averaged density, where $T_e(0)$ is the central electron temperature measured by ECE and V is the plasma volume.

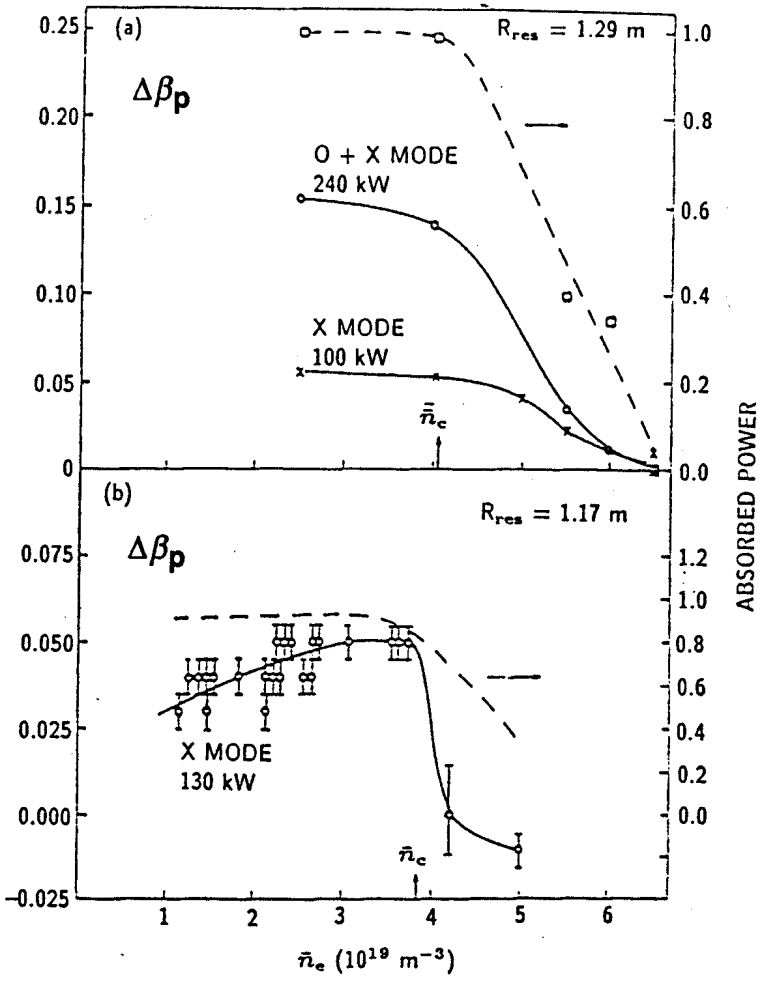

Fig. 7 - The increase in poloidal beta and the measured fractional absorption of heating power as a function of line-averaged density for DITE. The resonance is placed at (a) R_{res} = 1.29 m and (b) 1.17 m, compared to the major radius of 1.22 m. The wave is the X-mode launched from the high field side. The calculated cut-off densities are shown as $\bar{n}_c$.

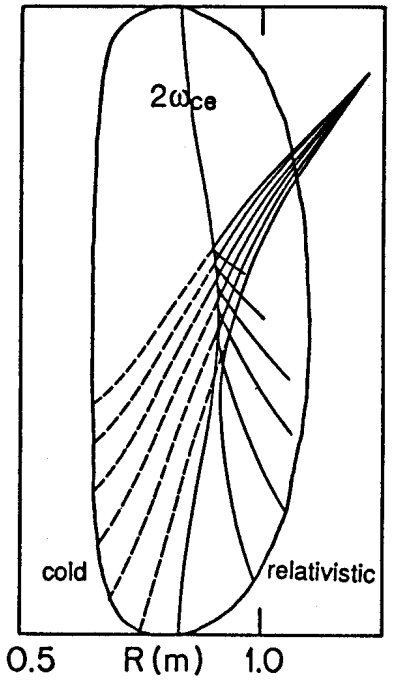

Fig. 9 - X2 oblique launch on a TCV elongated plasma for cold and relativistic dispersion (1 keV, $2 \times 10^{19} m^{-3}$). The knees at the resonance are sharper at low temperature, but disappear in the cold calculation.

Therefore, important additional refraction at the resonance is expected for important absorption at the resonance. This has for example important consequences for ray tracing for TCV X2 launch, where the rays can reflect off of the resonance for shallow launch before reaching the absorption layer and in this way lose much power deposition [13] (Fig. 9). In most ECRH experiments, microwave beams are launched close to normal to the resonance, reducing the consequences of these effects and justifying cold ray tracing calculations for these earlier experiments.

The changes to the index of refraction in the region of the harmonic resonances due to this effect is exemplified in the CMA diagram of Fig. 10b) [14] for X-mode and "relativistic" perpendicular ($\underline{k} \perp \underline{B}$) propagation. The effects on the n = 2 and n = 3 harmonics are clearly seen and explain the "relativistic" traject-ories occuring at shallow incidence in Fig. 9. Figure 10a) shows the cold case for reference.

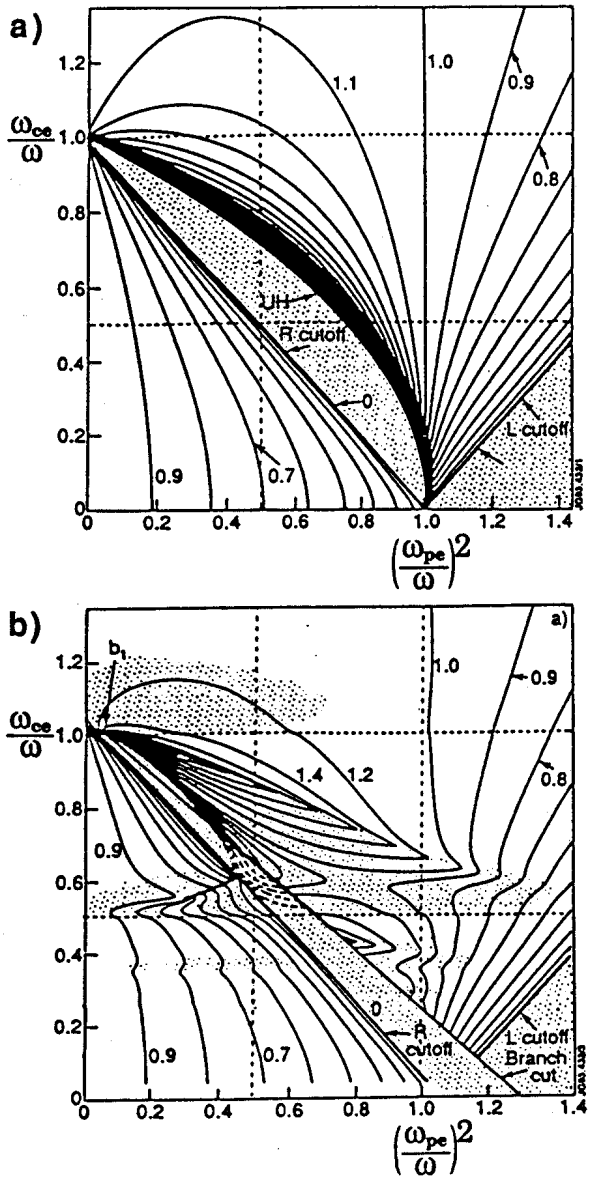

Fig. 10 - a) Contour plot of the refractive index N obtained with the cold model, in the CMA parameter space, for X-mode propagating perpendicular to the magnetic field. The distance between the contour levels is 0.1. An imaginary part in the refractive index only appears when Re(N) = 0 and is here marked by a dotted background.
b) Contour plots of the real part of the refrac-tive index, Re(N). The plots are obtained with the weakly relativistic model for X-mode pro-pagation perpendicular to the magnetic field for T_e = 15 keV. The steps between the contour levels are 0.1 for -1 < Re(N) < 1 and 0.2 for 1 < Re(N). For Re(N) < 0 the contour lines are broken. Regions with significant damping, Im(N) > 0.01, are marked by a dotted background. Because of the Riemann structure in the surface two branch cuts have been laid into the plot.

3. ECRH AS A TOOL IN TOKAMAKS

3.1 Breakdown and Assisted Startup

The loop voltage at startup in a large tokamak such as ITER is restricted to very low values: $E_\phi \leq 0.3$ V/m. The reason is that the vacuum vessel must be sufficiently strong to withstand the large forces associated with a disruption and therefore must be constructed without any insulating gaps. The need for a superconducting primary coil imposes a further limit on E_ϕ. ECH assisted Ohmic (OH) startup is the best method found to date to obtain reliable startup at reduced E_ϕ. It is efficient and has considerable tolerance to variation in prefill gas pressure and to magnetic field errors.

In TCA, startup has been obtained down to 0.15 V/m, a value typically 10-20 times lower than that required for reliable Ohmic breakdown in TCA. Thus values half of the required value for ITER have been achieved in TCA.

Experiments in TCA support the importance of the UH resonance for power deposition in the cold pre-ionisation plasma before significant plasma is present, see Fig. 4. Absorption both in the EC and UH resonances broadens the conductive channel and therefore lowers the inductance, which is favourable for effective ramp-up of the current. O-mode, due to incomplete first-pass absorption with multiple wall reflections and resulting mode conversions at the wall, produces broader current profiles than X-mode, due to a better distribution of the power on two resonances [6].

3.2 Heating and H-mode

Efficient electron heating by EC waves has been demonstrated in many experiments, both at the fundamental and 2nd harmonic resonances with nearly single pass absorption in medium-sized tokamaks.

Tokamaks with experimental results at injected ECH power above 0.5 MW are listed in Table I. (A list of all ECH experiments cited in this paper is given in annex, Table III).

Using LFS injection perpendicular to the magnetic field, a scheme which gives the best localisation of the heating over a radial extent of typically a few centimetres and favours bulk heating, high central electron temperatures have been reached. The electron temperature has exceeded 10 keV in T-10, with 2 MW ECRH at $\bar{n}_e = 1.5\times10^{19}$ m^{-3} [15]. Electron temperature profiles measured with Thomson scattering show very high values of T_e gradients (up to 50 keV/m) in a narrow central region [11], even at modest ECRH power levels. This indicates that in the central plasma region confinement degradation is small and indicates that efficient ignition of a Reactor may be possible using ECRH to heat the core.

Tokamaks	injected power [MW]	frequency [GHz]	mode	launch	$\bar{n}$ [$10^{19}m^{-3}$]	Refs.
T-10	~3	75-84	O-mode	LFS	5.5	[15]
DIII-D	1.4	60	O,X/X2	LFS HFS	3.4/1.5 4.5*	[8] [16]
COMPASS-C	0.75	60	X2	LFS	1.3	[17]
TFR	0.5	60	0	LFS**	2.2	[11]

* *"Overdense heating" is observed above this density. The heat is then deposited in the outer regions where the density is below cutoff, probably after reflections.*

** *The non-absorbed power fraction was mainly re-launched from the HFS in X-mode, using a mode converting mirror.*

Table I: Some of the tokamaks in which high power ECR Heating studies have been performed. The injected power level is the maximum power available for injection. The power is launched from the LFS or from the HFS. The average densities given are the maximum densities for which the power is well absorbed (single pass).

Recent high resolution Thomson scattering measurements in RTP are beginning to resolve details of the central T_e profile, showing narrow high temperature peaks, see Fig. 11 [18]. These filamentary structures explain, a posteriori, the important scattering in core electron temperature data obtained with coarser spatial resolution measurements. With the spatial resolution of the measurements in Fig. 11, local temperature gradients up to 1 MeV/m have been observed.

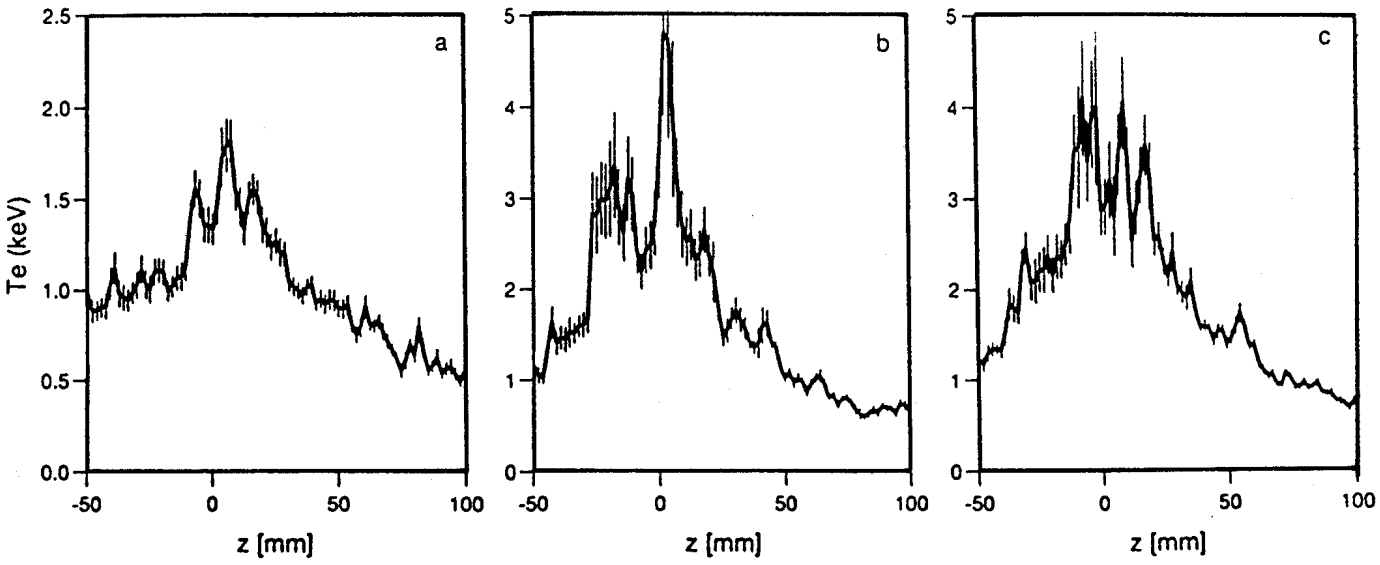

Fig. 11 - Examples of T_e profiles in RTP during the ECH pulse measured by high resolution Thomson scattering and showing distinct filamentation in the central plasma. a) q_a = 10; b) q_a = 5.2; c) q_a = 3.2. The limiter is at z = 165 mm.

ECRH directly heats electrons. Until now high power heating experiments in tokamaks have been conducted at frequencies below 84 GHz, and at the operating densities (which must be below the cutoff density for the given frequency) where electrons and ions were generally

decoupled since the electron-ion equipartition time exceeded the energy confinement time and ECRH had little effect on the ion temperature. In the next generation of ECRH experiments (for example in FTU and Tore Supra with frequencies up to 140 GHz and a cutoff density of 2.4×10^{20} m^{-3}) this limitation will be removed and ions will be heated.

3.2.1 Localisation of the Heating

With regard to where the heat is deposited in the plasma, which is different from where the power is absorbed, there are some differences between results from DIII-D and other tokamaks. In DIII-D, heating outside the centre (and up to at least $|r_{res}/a| < 0.8$), see Fig. 12, has an efficiency close to that of central heating; a huge inward heat-pinch is deduced from transport analysis of these experiments [19].

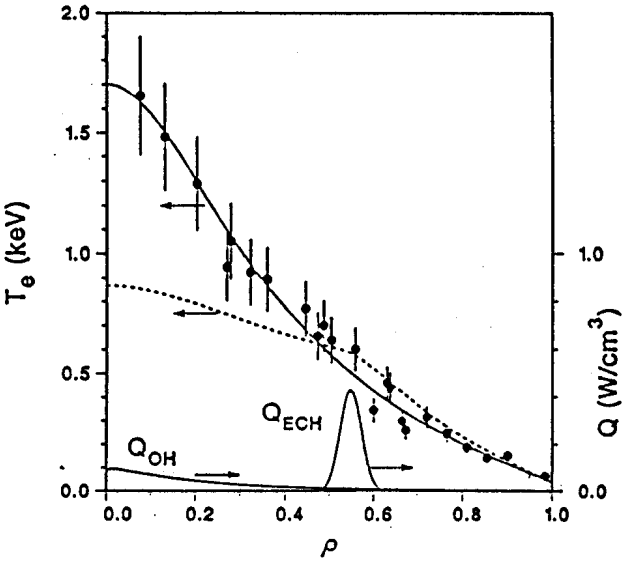

Fig. 12 - Experimental electron temperature profile as a function of the radial magnetic coordinate ρ measured by electron cyclotron emission and Thomson scattering. The plasma parameters are $\overline{n} = 2.2\times10^{19}$ m^{-3}, $B_T = 1.7$ T, plasma current I = 600 kA, and $P_{ECH} = 1.25$ MW. The calculated power deposition profile for the ECH is also shown. The dashed curve is a simulation with diffusive transport only.

Apparently, confinement in the edge region is better in DIII-D than in the other ECR heated tokamaks. In other experiments (notably TFR [11]) the heating efficiency is reduced when heating outside the q = 1 surface (this could be associated with the observed increase in levels of MHD activity). In T-10 the initial heating efficiency remains high as long as $|r_{res}/a| < 0.5$, but after a settling time the confinement time degradation is much worse than for central heating [20]. If some central heating is added (using a gyrotron at a different frequency), the efficiency of heating at $r_{res}/a \sim 0.5$ increases (to about half the efficiency of central heating). In all tokamaks it is observed that the MHD activity (sawteeth, m = 2, ELMS) can be affected by localised power deposition and this can have some additional effect (~ 20%) on the confinement time τ_E, therefore on heating efficiency.

3.2.2 H-mode

Experiments in DIII-D have demonstrated that ECRH is at least as efficient as neutral beam injection (NBI) in generating a transition to the high confinement, so-called H-mode [8]. At equal power levels the transition occurs sooner in ECRH, probably because in the NBI case a delay occurs due to the slowing down time necessary for energy input

from fast ions. The threshold power is independent of the localisation of power deposition.

H-mode transitions obtained with ECRH have also been demonstrated in the JFT-2M tokamak. Here the most efficient transition is obtained by directly heating the edge [21]. However the method decreases the central heating efficiency. Although the present paper only addresses tokamak work, it is the place to mention that the first H-mode reached in a stellarator was obtained with ECRH at 140 GHz [22] and, more recently, also at 70 GHz.

3.3.3 Confinement

Confinement under ECRH is too vast a subject to be addressed here. Let us remember that at modest ECRH power levels ($P_{ECRH} \lesssim P_\Omega$) several experiments report regimes where the energy confinement hardly changes from its Ohmic value or even improves. This may be related to the power deposition profile being more peaked than Ohmic profiles and to the relatively good confinement in the central region.

In heating experiments where relatively high ECRH powers have been applied ($P_{ECRH} >> P_\Omega$) at densities where the electron velocity distribution remains Maxwellian, confinement degradation is observed as with other additional heating.

As the frequencies of available gyrotrons increases, so does the accessible density range. The strong density dependence of the confinement time obtained earlier in low density experiments seems to decrease and to converge to the ITER-P-89-L scaling law value [16].

It should also be mentioned that the good localisation of ECRH power deposition in the discharge permits the use of power modulation techniques to extract heat diffusivity from the analysis of perturbed temperature profiles.

3.4 Local Profile Control to Influence MHD Properties

ECRH is able to provide local control of the pressure and current profiles via heating and current drive, and thereby to influence the MHD behaviour of the discharge.

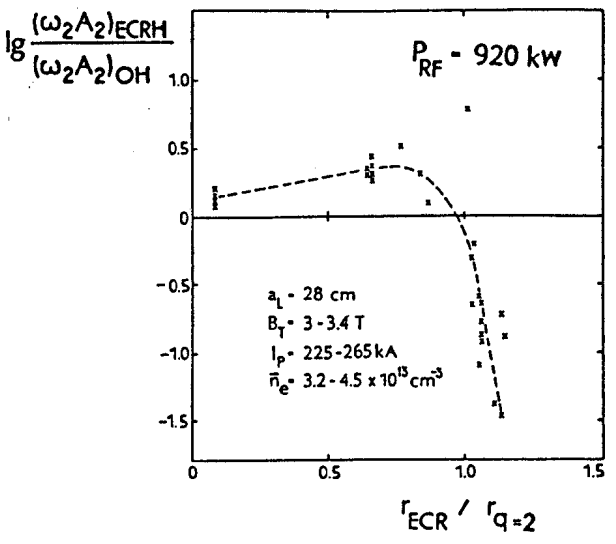

Several experiments in which ECRH is a substantial fraction of the input power have successfully demonstrated *reduction and suppression of m = 2 instabilities* for instance in T-10 [23]. In Fig. 13, the stabilisation is achieved by heating outside of the q = 2 radius, where the island is located.

Fig. 13 - Logarithmic plot of relative m = 2 oscillation envelope against relative radius of resonant zone.

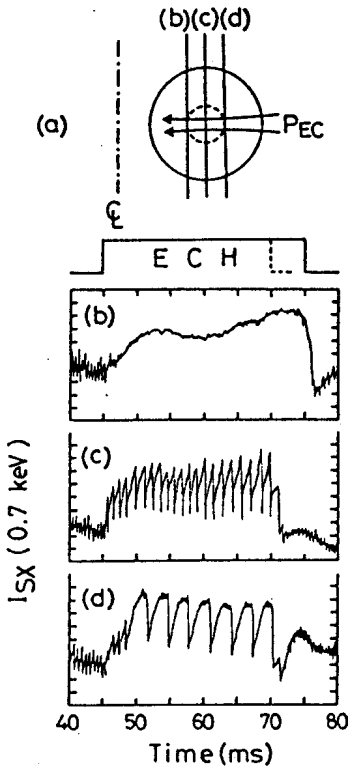

Fig. 14 - (a) Schematic of the wave trajectory and ECH layers r_{ECH} shown as vertical lines for the three cases (b), (c) and (d) shown here. The q = 1 surface is shown as a dashed circle. Evolution of the soft X-ray signal I_{SX} for (b) ECH at q = 1 on the high-field side (B_T = 0.93 T), (c) on-axis heating (B_T = 1.02 T), and (d) on the low-field side of q = 1 (B_T = 1.08 T), for q_L = 3.4, I_p = 83-100 kA, and P_{ECH} = 213 kW.

ECRH has been shown to *modify sawtooth behaviour* in several tokamaks with heating powers of the order of or greater than P_Ω. Off-axis heating near the q = 1 surface increases the sawtooth period or stabilises sawteeth completely, with the strongest effects at high power and/or low density, whereas on-axis heating tends to decrease the period. With second harmonic heating in WT3, stabilisation is generally easier when heating to the HFS of the magnetic axis compared with heating to the LFS, at $R_o < R - r_{q=1}$ compared with $R > R_o + r_{q=1}$, see Fig. 14 [24].
This suggests that the stabilisation is due to flattening of the current profile due to a local increase in the conductivity outside the q = 1 surface, but with a smaller increase in conductivity for $R > R_o + r_{q=1}$ due to stronger trapped particle effects.

Another example of the effect of a local control of pressure, temperature or current profile on the MHD behaviour is the effect of edge localised heating on the ELM's (Edge Localised Modes) in H-mode plasmas. This has been investigated in DIII-D [8], where, by changing the location of the resonance, the ELM frequency was changed. Using 1 MW of ECRH injecting X-mode from the high field side (single pass absorption 20-40%) into an NBI (5 MW) sustained H-mode plasma, the ELM frequency could be reduced by a factor of 4 when the resonance was outside the separatrix. Edge localised ECRH could, therefore, be useful as a means to strike the best balance between the negative (reduced confinement) and positive (purification) effects of ELMs.

3.5 ECRH on the CRPP TCV tokamak

The TCV objective is to study the influence of *elongation* and *strong shaping* on tokamak performance. In particular, the experimental programme will concentrate on the creation and control of highly elongated plasmas ($\kappa \equiv b/a \leq 3$, R/a=3.7, B=1.43T), on the study of their *operational limits* and on their *confinement* properties.

As a consequence both of the large variety of possible plasma configurations and because of its *flexibility*, ECRH is the most suitable

heating system for the TCV tokamak. All plasma shapes, including those with high elongation, can be heated using rotatable mirrors. In addition, the localization of the energy deposition possible with ECRH can be used for *modification of the current profile* (through control of the electron temperature profile) and hence for the creation of the broad current profiles necessary for vertical stability at high elongation. An ECRH pulse length of 2 s has been chosen so as to be of the same magnitude or greater than current diffusion times.

For the EC frequencies, the choice of extraordinary propagation modes in second X2 (82.6 GHz) and third X3 (118 GHz) harmonics permits heating at the nominal toroidal magnetic field (1.43T) in a high density plasma. With cutoff densities of 4.3 and 11.5×10^{19} m^{-3} respectively, combined X2 and X3, heating at fields between 90% and 100% of the nominal value is possible at high elongation. A power of 3 MW in X2 and 1.5 MW in X3 is planned.

Ray-tracing calculations of the resonance accessibility from the various TCV ports with realistic beam divergence have been performed using the TORAY code [25,13], which use weakly relativistic description for both dispersion and absorption. Accounting for plasma configurations from circular to fully elongated and imposing various density profiles, these calculations lead to the selection of horizontal to oblique lateral launch for *X2 heating and current drive* and quasi-vertical top launch for *X3 high density heating.*

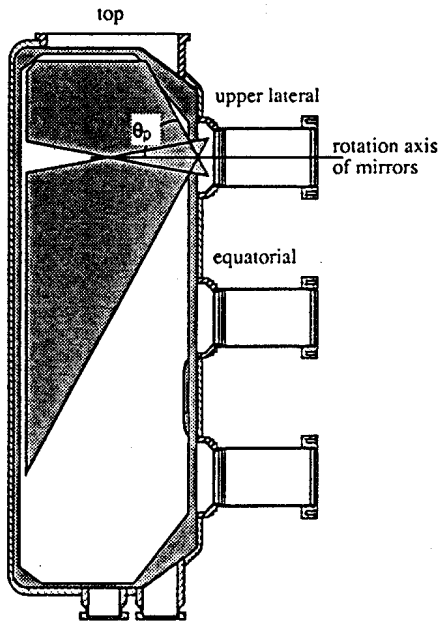

X2 heating: Wave power in X2 can reach any region of the plasma when launched from the upper lateral ports, since room for mirror adjustment permits a wide range of poloidal launch angles, see Fig. 15. The EC power is nearly 100% first-pass absorbed and can be deposited in the central region (defined loosely by the region where $x \equiv r/a \leq 0.4$) if the density is below cut-off on axis, even taking into account the "relativistic" effect on the trajectories shown in Fig. 9. By adjusting the mirror, the power launched from the same upper lateral ports can efficiently be absorbed close to the plasma edge, making it appropriate for *profile control.*

Fig. 15 - X2 upper lateral launch with the range of possible poloidal angles accessible for heating. By rotating the launcher around its axis, the same range of toroidal angles is available for CD. TCV will be equiped with 4 upper lateral and 2 equatorial X2 launchers.

X3 heating: In contrast to X2, X3 is launched from a port at the top of the vessel giving a beam path quasi-parallel to the resonance, Fig. 16a). This results in geometrically enhanced first-pass absorption, even for mildly elongated plasmas. Launched from the top port, X3 power results in efficient central deposition for a broad range of density. With a moderate elongation, $\kappa=2$, and density $n_{eo} \leq 7\times10^{19}$ m^{-3}, first-pass absorption of 60% is achieved in an Ohmically heated plasma (see Fig. 16b) and is more than 95% absorbed in a supplementary heated plasma (admitting $T_e \sim 2\times T_{eOH}$). For full elongation $\kappa=3$, first-pass absorption increases to 80% and 100%, respectively.

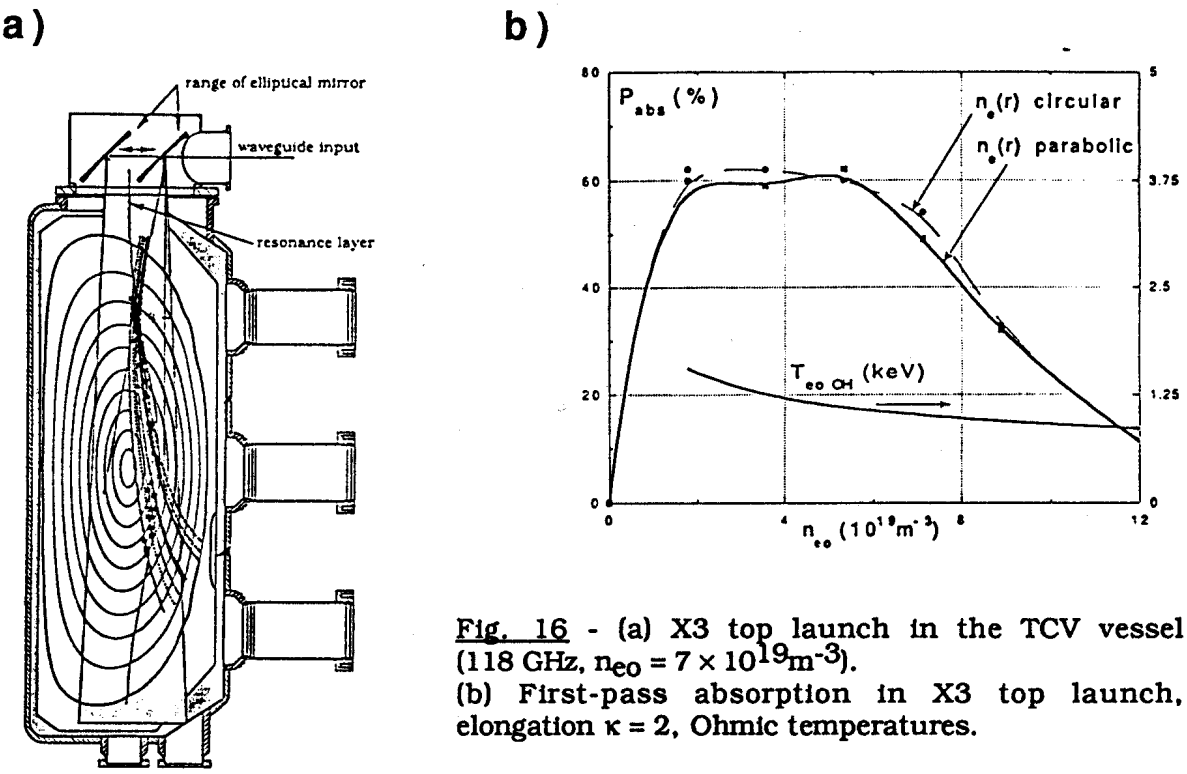

Fig. 16 - (a) X3 top launch in the TCV vessel (118 GHz, $n_{eo} = 7 \times 10^{19}$m^{-3}).
(b) First-pass absorption in X3 top launch, elongation $\kappa = 2$, Ohmic temperatures.

4. TOWARDS THE REACTOR

A rich variety of applications exists for ECRH - (some of which can be carried out by other heating methods, such as Lower Hybrid (LH), Ion Cyclotron (IC), or Neutral Beam Injection (NBI)). However, it should be stressed that ECRH shows *no problem in coupling power to the plasma through a vacuum layer*, that *no increase in impurity levels is induced by interaction with the antennae* and that the *barrier window can be placed remotely behind a radiation shield*. EC waves are suitable for *direct electron heating*. *Accessibility to the internal plasma regions* is possible as long as the density is below the cutoff density. The spatial absorption profile is localised and for operation conditions typical for a Next Step tokamak, *total absorption* in any part of the discharge is possible by choosing the appropriate frequency and injection angle. For heating purposes very simple launching systems with high power throughput can be used,

which in a Next Step device can be simply *dog-legged* through the blanket using mitre bends, thus reducing neutron escape through the blanket. Oversized waveguides with power densities up to *700 MW/m²* in vacuum and half that value at atmospheric pressure have already been used.

A particular strength of ECW is their effectiveness in *assisting plasma initiation at low loop voltage*. For breakdown (BD) and startup applications in ITER, an ECRH power of 5-10 MW [26] or possibly 20 MW or more [27] seems to be needed. Therefore further comparison of experiments and simulations are required to better assess the power needed for BD and initial shaping of the current profile in the startup phase of ITER.

Control of the burn temperature can be covered by electron cyclotron waves. A power of 50 MW is more than sufficient according to the Rebut-Lallia-Watkins transport model. Frequencies in the range of 150 to 170 GHz are needed. Control of the absorption profile requires varying the frequency and/or the angle of injection.

The *current drive* efficiency $\gamma = \langle n_e \rangle I_{CD} R / P_{RF}$ is about 0.2×10^{20} A/Wm^2 in the core plasma, decreasing to still much lower values in the outer parts of the discharge as a consequence of the presence of a large population of trapped electrons [5]. For central CD, frequencies in the range of 180 to 220 GHz are needed with toroidal launch angles of 35°-40° from normal incidence, yielding typically I_{CD} = 1 MA for 50 MW of injected power ($n_{eo} = 1.4\times10^{20}$ m^{-3}, T_{eo} = 20 keV). This current drive efficiency is quite satisfactory for generating a "seed" current in the plasma centre. For comparison, other CD methods exhibit similar efficiencies: LHCD yields typically 0.3-0.5×10^{20} A/Wm^2 and ICCD yields about 0.2-0.5×10^{20} A/Wm^2 depending on the heating scheme. The good localisation of ECCD power deposition and the efficiency value of ECCD constrains ECCD for *local plasma current profile control* applications around the q=2 magnetic surface, for which 40 MW at a frequency of 140 GHz is needed.

There has been continued development of ECRH technology in the past years. This development has continued along two main lines of microwave sources: the gyrotron and the free electron maser (FEM). In both cases, the energy of an accelerated electron beam is transformed into microwave power, in a resonant cavity for a gyrotron and in a spatially modulated static magnetic field (wiggler field) for a FEM. The present state of the art of gyrotron development is shown in Table II [28], where the gyrotron with characteristics 167 GHz, 500 kW, 0.7 s represents today the best achievement in the direction of ITER sources.

In Europe, the FEM line is developed at FOM, The Netherlands, producing a tuneable 130-260 GHZ microwave beam at 1 MW.

References

[1] A.C. England, IEEE Trans. on Plasma Science, **PS-12** (1984)124.
[2] H. Bindslev, Plasma Physics and Contr. Fusion **34** (1992) 1601.
[3] H. Bindslev, Plasma Physics and Contr. Fusion **35** (1993) 1093.
[4] D.F.H. Start, M.R. O'Brien and P.M.V. Grace, Plasma Phys. **25** (1983) 1431.
[5] V.V. Alikaev and V.V. Parail, Plasma Phys. and Contr. Fusion **33** (1991) 1639.
[6] D.R. Whaley, T.P. Goodman, A. Pochelon et al., Nucl. Fus. **32** (1992) 757.
[7] A.H. Kritz, H. Hsuan, R.C. Goldfinger, D.B. Batchelor. Proc. of 3rd Joint Varenna-Grenoble Int. Symposium on Heating in Toroidal Plasma (Euratom Report EUR 7979 EN, 1982), Vol. II, 707.
[8] R. Prater, N.H. Brooks, K.H. Burrel, et al., Proc. of 12th Int. Conf. on Plasma Physics and Contr. Nucl. Fus. Res., Nice, Vol. I (1988) 527.
[9] M. Ashraf, R. Barnsley, N. Deliyanakis, et al., ibid. Vol. I (1988) 541.
[10] M. Bornatici, R. Cano, O. de Barbieri, F. Engelmann, Nucl. Fus. **23** (1983) 1153.
[11] TFR-Group and FOM-ECRH-Team, Nucl. Fusion **28** (1988) 1995.
[12] F. Smits et al. Proc. 18th EPS Conf. on Contr. Fus. and Plasma Heating, Berlin (1991).
[13] A. Pochelon et al., 20th EPS Conf. on Contr. Fus. and Plasma Physics, Lisboa, Vol. 17C, Part II (1993) 1029.
[14] J. Egedal and H. Bindslev, JET Preprint JET-P(93)74, Plasma Phys. and Contr. Nucl. Fusion, **35** (1993) 543.
[15] V.V. Alikaev et al. 11th Int. Conf. on Plasma Physics and Contr. Nucl. Fusion Research, Kyoto (1986) Vol. 1, 111.
[16] T.C. Luce et al., 13th Int. Conf. on Plasma Physics and Contr. Nucl. Fusion Research, Washington (1990) Vol. 1, 631.
[17] P.G. Carolan et al., Proc. 18th EPS Conf. on Contr. Fusion and Plasma Heating, Berlin, Vol. 15C, Part I (1991) 81.
[18] N.J. Lopes Cardozo, F.C. Schüller, C.J. Barth et al., submitted to Phys. Rev. Letters.
[19] T.C. Luce, C.C. Petty and J.C.M. de Haas, Phys. Rev. Lett. **68** (1992) 52.
[20] V.V. Alikaev, A. Bagdasarov, E. Berezovskii et al., Plasma Phys. and Contr. Fusion **29** (1987) 1285.
[21] K. Hoshino et al., Phys. Rev. Letters **63** (1989) 770.
[22] V. Erkmann, R. Brakel, R. Burhenn et al., 14th IAEA Conf. on Plasma Phys. and Contr. Nucl. Fus. Res., Würzburg, Vol. II (1992) 469.
[23] V.V. Alikaev, Yu.I. Arsentiev, A.A. Bagdasarov, et al., Plasma Phys. and Contr. Fus. Res. (IAEA London 1984), Vol. II (1985) 419.
[24] K. Hanada et al., Phys. Rev. Lett. **66** (1991) 1974.
[25] R.C. Myer, M. Porkolab, G.R. Smith, A.H. Kritz, Nucl. Fus. 29 (1989) 2155.
[26] G.V. Pereverzev et al., ITER-IL-PH-6-9-E-2 (1990).
[27] C. Maroli and V. Petrillo, Report PM-89-005 (1989).
Final Report of NET Contract Nr. 179/84-12/FU-I.
[28] M.J. Petelin, Plasma Phys. and Contr. Nucl Fusion **35** (1993) B 343.

Device	R (m)	a(m)	b/a	B(I)	I_p (KA)	Frequency (GHz)	Power (MW)	EC Pulse length (s)	Scheme	Aim/results
Compass-C	0.56	0.22	1.73	2.1	400	60	0.75 (2)	5	X2	Heating and CD
DIII-D	1.68	0.62	1.7	2.2	3.5 MA	60 110	1.4 (2) 2	0.75 10	0/X HFS, X2 LFS X2 LFS	Heating and CD, Plasma formation Heating and CD
DITE	1.22	0.30	1	< 2.8	200	60	0.6	0.2	01 LFS (CD: X1 HFS)	Heating and CD
ITER*	7.75	2.80	1.6	6	25 MA	110-180* 150* 120-5.155±5* 180-200*	5-10 50 20-30 70-150 a few ×10MW	.5-few sec		Plasma formation Plasma heating to ignition Plasma stabilisation Global ECCD Local ECCD
JFT-2M	1.31	0.35	1.6	1.5	550	59.8	0.23 (0.5)	0.1	X2 LFS	H-mode
RTP	0.72	0.17	1	< 2.4	< 150	60 110*	0.36	0.1	01 LFS - X1 HFS	Heating, transport, plasma formation
T-10	1.50	0.25-0.39	1	3	250	75 84 (81.3 for CD)	~3 total		01 LFS	Heating, CD, Plasma formation
TCA	0.61	0.18	1	1.5	175	39	0.16	0.20	01/X1 HFS	Plasma formation, heating
TCV	0.88	0.24	3	1.5	1 MA	39* 82.6* 118*	0.25 3.0 1.5	0.20 2 2	01 LFS X2 LFS X3 TOP	Plasma formation Heating, curent profile shaping, CD Heating, β-limits
TFR	0.98	0.20	1	4-6	400	60	0.5	0.1	01 LFS (twist mirror on the HFS)	Heating
Thor	0.52	0.17	1	1	100	28	0.08-0.013	0.005-0.01	01 LFS (twist mirror on the HFS)	Plasma formation
Tore Supra	2.36	0.80	1	4.5	2 MA	118*	2	210 (sic)	01 LFS	Synergy with LHCD
W7-AS	2.0	0.18	-	2.5	-	70 140	1.2 0.5	3 0.5	01 LFS X2 LFS	Plasma formation, CD and H-mode
WT-3	0.65	0.20	1	<1.75	160	56	0.2	~0.025	X2 LFS	Sawtooth stabilization

Table III: Tokamak cited in this paper with ECH-system characteristics. As much as possible, the data are given for conditions close to the experiments mentioned (*: projected experiment)